Combining Ganglion Cell Topology and Data of Patients with Glaucoma to Determine a Structure–Function Map

Andrew Turpin,[1] *Geoff P. Sampson,*[2] *and Allison M. McKendrick*[2]

Purpose. To introduce techniques for deriving a map that relates visual field locations to optic nerve head (ONH) sectors and to use the techniques to derive a map relating Medmont perimetric data to data from the Heidelberg Retinal Tomograph.

Methods. Spearman correlation coefficients were calculated relating each visual field location (Medmont M700) to rim area and volume measures for 10° ONH sectors (HRT III software) for 57 participants: 34 with glaucoma, 18 with suspected glaucoma, and 5 with ocular hypertension. Correlations were constrained to be anatomically plausible with a computational model of the axon growth of retinal ganglion cells (Algorithm GROW). GROW generated a map relating field locations to sectors of the ONH. The sector with the maximum statistically significant ($P < 0.05$) correlation coefficient within 40° of the angle predicted by GROW for each location was computed. Before correlation, both functional and structural data were normalized by either normative data or the fellow eye in each participant.

Results. The model of axon growth produced a 24-2 map that is qualitatively similar to existing maps derived from empiric data. When GROW was used in conjunction with normative data, 31% of field locations exhibited a statistically significant relationship. This significance increased to 67% (z-test, $z = 4.84$; $P < 0.001$) when both field and rim area data were normalized with the fellow eye.

Conclusions. A computational model of axon growth and normalizing data by the fellow eye can assist in constructing an anatomically plausible map connecting visual field data and sectoral ONH data. (*Invest Ophthalmol Vis Sci.* 2009;50:3249–3256) DOI:10.1167/iovs.08-2492

As methods become available to measure the structure of the retinal nerve fiber layer (RNFL) and optic nerve head (ONH), several techniques have emerged to map the location of visual sensitivities obtained by automated perimetry in the 24-2 pattern to sectors of the ONH.[1,2] Figure 1 shows the map published by Garway-Heath et al.[1] that is used in most current studies on the structure–function relationship in glaucoma. Each location in the visual field is mapped to one of six sectors on the ONH. We will refer to this as the G map throughout this article.

Such maps are valuable in current research conducted to relate the structural loss due to glaucoma with functional loss, to better understand the glaucomatous process.[1,3] Moreover, accurate maps tailored to an individual can potentially lead to new developments in diagnostic tools, such as fundus and scotoma oriented perimetry,[4] in which structural measures such as Heidelberg Retinal Tomography (HRT; Heidelberg Engineering, Heidelberg, Germany) or retinal photography can inform stimulus placement for functional testing.

The G map extended previous partial maps[5–7] and was derived by hand labeling composite digital images of retinal photographs and the 24-2 visual field pattern in 69 eyes with normal-tension glaucoma.[1] RNFL defects were traced back to the ONH, and the entry point of that path was recorded as an angle from the temporal margin for any of the 24-2 locations that were adjacent to the defect. The decision on sector boundaries was then made as a compromise between the SD of the angle for each location from the various eyes (median 7.2°) and the number of data points that were available for each sector.

In their two papers, Anton et al.[6] and Yamagishi et al.[7] introduced the idea of normalizing rim area measurements to account for changes in disc size between patients. They document some seeming correlations between focal disc and focal field defects in two small cohorts of patients by using 10° sectors of HRT data.

A less labor-intensive approach to producing a map was taken by Gardiner et al.[2] In that study, statistical correlations were obtained between visual field data (Humphrey Field Analyzer [HFA] 24-2; Carl Zeiss Meditec, Dublin, CA) and rim area produced by the Heidelberg Retinal Tomograph (HRT) divided into 36 possible sectors on a group of 166 eyes from people with ocular hypertension, early glaucoma, or suspected glaucoma. The rim area measurements were normalized against disc area of the same eye before computing correlations. While not requiring the manual labeling of defects used in previous studies, the correlation approach of Gardiner et al. also produced many correlations that are probably not meaningful for establishing a relationship between stimulus location and ONH sector. Moreover, the strongest correlations were quite low (correlation coefficient, ~0.35), reducing confidence in the relationships. A possible advantage of this approach, however, is that it removes the potential for confounds introduced by human error in assessment of disc and field measurements. A further advantage is that it can be easily applied to stimulus placement arrangements other than the 24-2 pattern.

In this article, we are interested in producing a map for the stimulus placement arrangement of the Medmont automated perimeter (M700; Medmont Pty., Ltd., Camberwell, VIC, Australia). The most commonly used tests of the Medmont perimeter (Central Threshold/Glaucoma Threshold) assess many more locations than the Humphrey 24-2 pattern—96 compared with 54—and samples the visual field in concentric rings, rather than in a rectangular grid. This increased sampling may enable enhanced resolution for the determination of the relationship between ONH structure and visual function in glaucoma. The secondary purpose of this work is to develop

From the [1]School of Computer Science and Information Technology, RMIT University, Melbourne, Victoria, Australia; and the [2]Department of Optometry and Vision Science, The University of Melbourne, Melbourne, Australia,

Supported by National Health and Medical Research Council (NHMRC) Grant 353567 (AMM) and ARC (Australian Research Council) Grant DP0558916 (AT).

Submitted for publication June 25, 2008; revised December 21, 2008; accepted May 11, 2009.

Disclosure: **A. Turpin**, None; **G.P. Sampson**, None; **A.M. McKendrick**, None

The publication costs of this article were defrayed in part by page charge payment. This article must therefore be marked "*advertisement*" in accordance with 18 U.S.C. §1734 solely to indicate this fact.

Corresponding author: Andrew Turpin, School of Computer Science and Information Technology, GPO Box 2476V, Melbourne, Victoria 3001, Australia; andrew.turpin@rmit.edu.au.

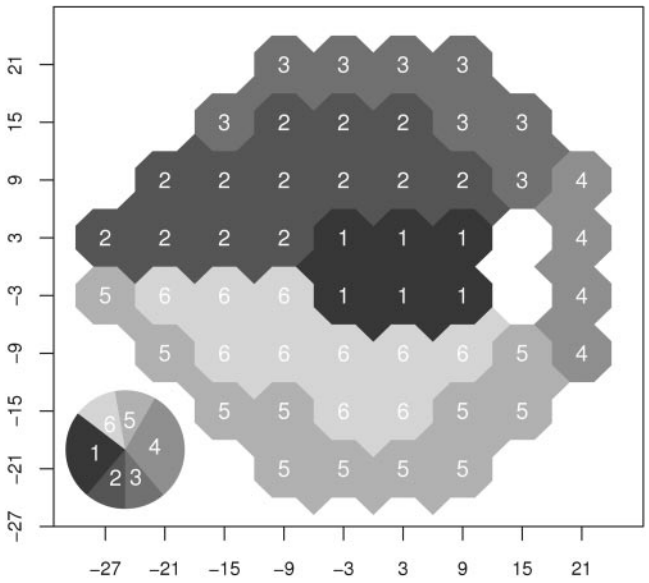

FIGURE 1. The G map of visual field location to the ONH for a right eye as published by Garway-Heath et al.[1] Numbers within octagons are centered on visual field locations of the 24-2 pattern and correspond to sectors of the ONH. The circle denotes the division of the ONH into the six sectors, with sector 1 being the temporal margin, sector 6 the superior–temporal, and so on.

improved methods for the determination of such structure–function relationships that can be applied more generally. Although the methodology described herein was applied to visual field data from the Medmont perimeter, it is entirely transferable to other visual field test patterns and stimuli.

Our methods begin with the approach of Gardiner et al.,[2] but we added two techniques to the method in an effort to reduce seemingly physiologically implausible relationships. First, we normalize both the functional and structural data with the fellow eye of each patient, rather than against the disc size of the same eye, or a normative database. The intuition was that gross anatomic features such as blood vessel placement and size and disc size and orientation are similar in each eye, as supported by the Bridlington Eye Assessment Project,[8] and so provide a good normalization factor for structural measures. Likewise, visual field sensitivity patterns (the hill of vision) should be similar in both eyes if normal; it has been shown that normalizing by the fellow eye can help in the detection of glaucomatous progression.[9] Then, we devised a model of axon growth in the eye which we used to limit the sectors with which a location can be correlated.

With the addition of these techniques, we get correlations that are physiologically meaningful and double the number of locations with correlations to the appropriate sector that are statistically significant ($P < 0.05$).

METHODS

Computer Model of Axon Growth

The sector of the ONH that is related to the location of a visual stimulus as it hits the retina is governed by the path that axons from the stimulated retinal ganglion cells (RGCs) take to exit the eye. Although much is known about the growth of RGC axons in utero, the exact mechanism is not well understood.[10] It is known that the axons grow from the RGCs across the retina and exit the eye through the ONH and that they tend to fasciculate together to form small bundles.[10] If we make the assumption that when axons develop they take the shortest path from the RGC to the ONH and that the eye is a sphere, we can immediately generate a location-to-sector map. Unfortunately, such a map does not bear much relation to our observations of the RNFL in the retina, as nearly all locations in the nasal visual field (both inferior and superior) are mapped to sector 1 of the G map in Figure 1.

Not only would this lead to a large number of axons tracking across the fovea, we know from RNFL thickness measurements of normal eyes[11] that the RNFL is thin at the temporal margin of the disc, relative to the superior and inferior areas. Hence, having more than half the RGCs underlying visual field locations with their axons exiting the eye in sector 1 of the G map is clearly incorrect. If this were the case, then the temporal margin would be the thickest part of the RNFL profile around the optic disc. We can alter the model to take this into account by imposing an order in which RGCs grow their axons, and then only allowing an axon into a certain sector if that sector is not already "full" of other axons according to the RNFL thickness profile around the disc. This also has the side effect of fascicularization: The axons tend to form bundles.

Figure 2 describes a simple algorithm (dubbed GROW) for realizing this model. To summarize, the ONH is divided into sectors, and the retina is divided into a grid of elements. The RGCs in each element attempt to assign their axons to the sector of the ONH that is closest along the surface of a sphere. If the sector is already "full" of axons, according to an RNFL thickness profile, then an alternate sector must be found. The order in which elements are chosen to grow their axons therefore is important, as elements chosen early in the process are likely to find room in their closest sector, whereas later elements are likely to have to find new sectors. Although the algorithm does not explicitly prohibit axons from tracking across the foveal pit, if elements are ordered according to their distance from a point midway between the fovea and the ONH, this effect happens automatically.

Information of the distribution of RGCs on the retina required for steps 1 and 5 in Figure 2 are taken from the data published by Curcio and Allen.[12] The profile of RNFL thickness required in step 2 is taken from Figure 4 in Hood and Kardon,[13] simply normalized to sum to 1 and assuming that on average the thickness of axons is roughly the same in each sector. In step 3, for the experiments reported herein, we use a hexagonal grid with each hexagon having a side length of 0.2 mm, and shorten the distance of each hexagon from the start point by a factor of 1.28 in the horizontal axis. This is based on the observation of Curcio and Allen[12] that the contours of RGC density follow an elliptical pattern, with the horizontal axis of the ellipse being 1.28 longer than the vertical on average.[12] We chose the starting point of the growth to be slightly to the ONH side of the fovea (−2.5°). The starting point is based in part on the knowledge that central RGCs grow their axons before peripheral RGCs,[10] and in part by the observation that RGCs close to the foveal side of the ONH would surely have axons that track directly into the ONH, and not in some arcuate path. This second claim is supported by the G map, where RGCs in sector 1 are all between the fovea and the ONH. We fix the position of the ONH at (−15°, 0°), and discuss possible ramifications of this in the final section of the paper. Finally, if steps 12 and 13 of GROW are reached—that is, the sector on the shortest path is full, and an alternate sector must be found—we search sectors in an order that respects the horizontal meridian. For example, if we are constructing a map with the six sectors of the G map and sector 6 is full, we try sector 5; and if sector 2 is full, we try sector 3. Although such a scheme does not explicitly prevent RGCs from having axons that cross the horizontal midline to enter the ONH, with the parameters chosen in this article, such a crossing does not occur. Also note that we are assuming that each RGC has a single axon entering the ONH, and so

$$\sum_e C_e = \sum_i S_i = R$$

where the parameters for this equation are defined in Figure 2.

1. Choose a total number of RGCs for the retina, R.
2. Divide R into the number of sectors chosen for the map using a RNFL thickness profile around the disc for normal eyes. Let S_i be the number of axons that can enter sector i, hence, $\sum_i S_i = R$.
3. Divide the retina into a grid of elements.
4. For each element e in order of increasing distance from a start point do
5. Let C_e be the number of RGCs in the element e.
6. Compute the shortest path from the middle of the element to the edge of the ONH, and determine the sector i where this path enters the ONH.
7. If $S_i > 0$ then record i as the sector for element e.
8. If $C_e \leq S_i$ then there is room in the sector for C_e axons so
9. Subtract C_e from S_i.
10. Otherwise
11. Subtract S_i from C_e and set S_i to zero; sector i is now full of axons.
12. While $C_e > 0$, there are still axons to assign to a sector so
13. Find another sector j with $S_j > 0$ for the remaining C_e axons and reduce S_j and C_e accordingly.

FIGURE 2. Algorithm GROW for assigning elements of the retina to sectors of the ONH.

Empiric Data

A total of 57 participants had visual fields measured with the Medmont perimeter M700 (Central Threshold or Glaucoma test) and HRT images taken. The Medmont perimeter is described fully elsewhere.[14] In brief, it is a fully automated, hemispheric bowl perimeter (300-mm radius), with a background illuminance of 10 apostilbs (3.2 cd/m^2). Stimuli are Goldmann size III (0.43°) targets that are LEDs of 565-nm wavelength that retroilluminate fixed points within the bowl. Thresholds are determined with a ZEST (zippy-estimation by sequential thresholding) procedure. Fixation performance is monitored by the Heijl-Krakau technique, and is continuously displayed to the operator. False-positive and -negative response rates are estimated in catch-trials interspersed throughout the test. For visual fields to be included in the study, the rate of response errors had to be less than 25%. Retinal tomography images were obtained on an HRTII machine (Heidelberg Engineering), but were exported using the HRT version III software. For inclusion, the standard deviation of the HRT images had to be less than 50 μm. Most participants had visual fields and ONH images measured on the same day; however, a time window of up to 3 months was permitted (median, 0 days; 95th percentile, 0 days; maximum, 88 days).

Thirty-four of the participants had an established ophthalmic diagnosis of primary open-angle glaucoma of which 29 were being treated bilaterally. Eighteen participants were classified as having suspected glaucoma because of having suspect ONHs. Five participants were classified as having ocular hypertension based on a clinical history of repeated intraocular pressure measures greater than 21 mm Hg. Participants were recruited prospectively from the Glaucoma Clinic of the Melbourne Optometric Clinic (Victorian College of Optometry) or were participating in other glaucoma-related psychophysical studies in the laboratory of one of the authors (AMM). All participants were required to have no history of ocular injury, to have refractive errors no greater than 5.00 D spherical and 2.00 D of astigmatism, and to have visual acuities no worse than 6/9. The study conformed to the tenets of the Declaration of Helsinki, and all participants provided written informed consent in accordance with a protocol approved by our institutional human research ethics committee before participation in the study.

Figure 3A shows the age distribution of the participants and the global indices for left and right eyes returned by the Medmont perimeter (Figs. 3B, 3C). The Medmont perimeter global indices are average defect (AD) and pattern defect (PD). These indices are similar but not

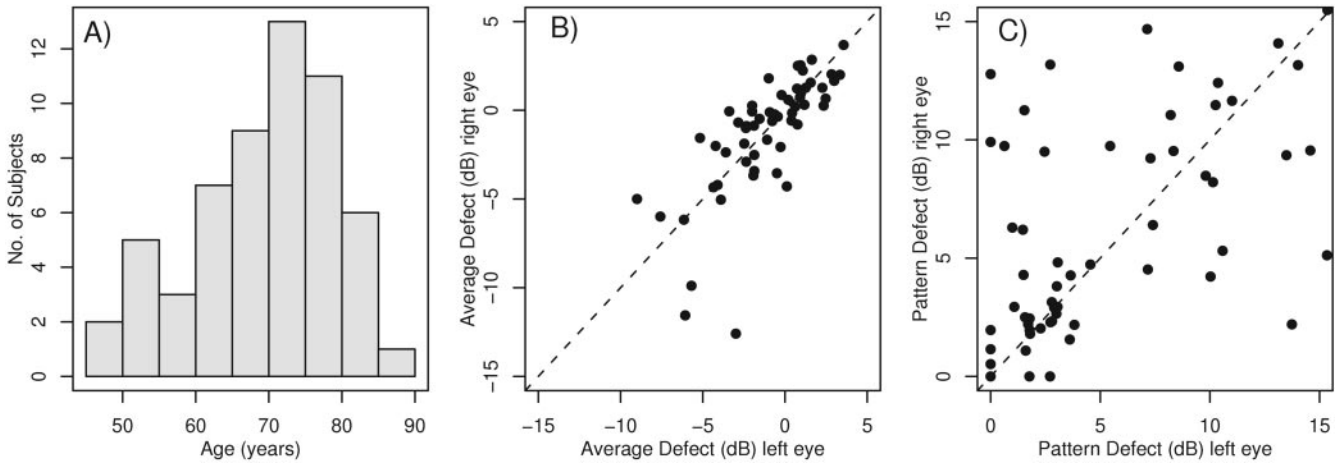

FIGURE 3. Demographics of empiric data: age of participants (**A**) and Medmont global indices for left and right eyes of participants (**B**, average defect; **C**, pattern defect).

Table 1. The Five Approaches to Computing Correlations between Sectors and Locations

Approach	Structural	Normalization	*P*	GROW
Basic	Rim Area	Gardiner et al.[2]	1.00	360°
Basic-p	Rim Area	Gardiner et al.[2]	0.05	360°
Basic-pg	Rim Area	Gardiner et al.[2]	0.05	40°
Fellow-A	Rim Area	Fellow eye	0.05	40°
Fellow-V	Rim Volume	Fellow eye	0.05	40°

P, the largest probability of the Spearman correlation allowed for the sector to count toward the maximum for a location. GROW, the maximum allowable distance of a sector from the angle predicted by Algorithm GROW for a sector to count toward a location.

identical with the mean deviation and pattern standard deviation indices of the Humphrey perimeter. A conversion factor between the Humphrey and Medmont perimetric indices has been published by Landers et al.[15]

Analysis

Our basic approach to identifying which sector of the ONH corresponds to which location in the visual field follows that of Gardiner et al.[2] We use 92 locations from the Medmont visual field, which are the 96 points that form the intersection between the central threshold and glaucoma threshold test patterns, excluding four locations around the blind spot. For each location, we compute correlation coefficients for left eyes between all thresholds at that location and normalized rim area measurements[2] for each of the 10° sectors output by the HRT software. All visual field data were corrected to age 45, using a correction of 1 dB per decade. The choice of left eye was arbitrary. The sector with the highest correlation coefficient is taken to be the sector related to that location.

In this basic approach there is no requirement for a correlation to be statistically significant at any level, nor is there any restriction on the anatomic plausibility of correlations between locations and sectors.[2] We then introduce two restrictions on the sectors that can be considered for any location: first, correlations must be statistically significant at the 0.05 level; and second, sectors must be within ±40° of the angle chosen for the location by the Algorithm GROW. Both choices are somewhat arbitrary, with 0.05 chosen simply by convention, and 40° chosen as one sector larger that the 95% confidence limit for the possible angles of entry into the ONH for a location in the participant group of Garway-Heath et al.[1] In addition to these two filters on the basic approach, we trialed a new normalization technique that subtracts the right eye data from the left before correlations were computed.

Table 1 summarizes our approaches.

Results

Model of Axon Growth

Figure 4A shows the map produced by our simple computational model of axon growth assuming 1.25 million RGCs in the retina,[12] and the six sectors used to generate the G map. A cursory look at this figure in comparison to Figure 1 shows that the maps are similar. Figure 4B shows the difference between the angles published with the G map[1] and the center of the sector chosen by our model run with 10° sectors. Under this more careful analysis, our map is very similar to the G map, with the major differences being around the (−27°, 3°) location and the (9°, −21°) location. These maximum differences, however, are of the order noted between eyes in Garway-Heath et al.,[1] where they reported a median standard deviation of 7° for angles. Hence, a difference of 30° between two locations would occur stochastically approximately 5% of the time. Given this fact, it seems that we have demonstrated that the computational model of axon growth we have developed is suitable for this mapping task.

The Medmont Visual Field

Figure 5 shows the results of computing the highest correlated sector for each location in the Medmont visual field using the basic approach. Note that while left eyes were used as input for this analysis, the figure is displayed in right eye format for ready comparison with the previous. All locations have an associated sector, except for the four points in the blind spot region. This is consistent with the results reported by Gardiner et al.[2] for the 24-2 pattern visual field. The correlation coefficients are low, ranging from 0.13 to 0.57 with a mean of 0.29, and there are some anatomically unexpected correlations. For example, the location near (22°, 6°) in Figure 5 has an angle of 340° indicating that it correlates with a sector on the temporal side of the ONH, rather than the nasal as might be expected. Similarly, the location near (−6°, 22°) has an angle of 30° indicating a superior sector of the ONH, when inferior seems more likely.

Insisting that the correlations must be statistically significant as in the Basic-p approach removes half of the points from the map, leaving 50 locations covered—53% of the field. The minimum correlation coefficient increases to 0.26, with the mean coefficient increasing to 0.33. This result is summarized in row two of Table 2. The mean correlation coefficients in Table 2 represent the average of different visual field locations for each of the approaches to allow comparison with previous work. We have not performed statistical tests to determine

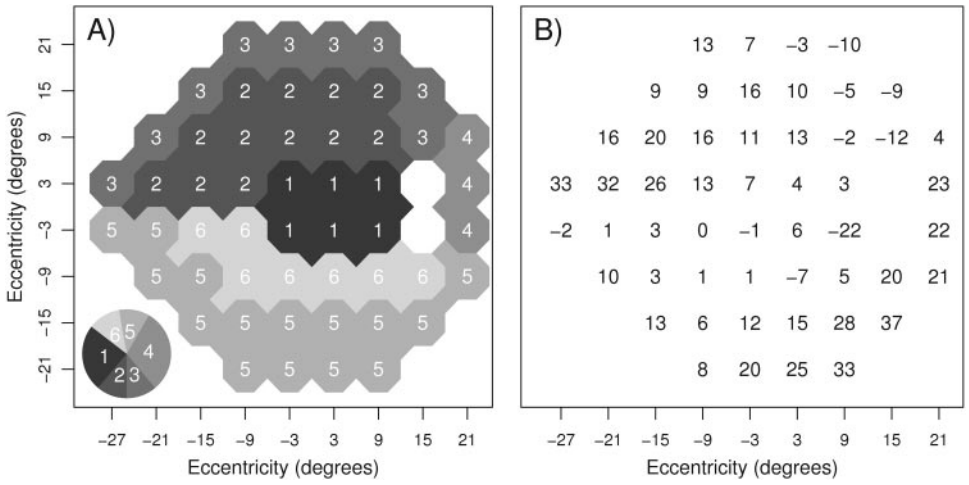

Figure 4. The map of visual field location to the ONH as determined by our computational model of axon growth. (**A**) The sector map in the same format as Figure 1. (**B**) The difference between mean angles (degrees) of the G map as published and the middle of our predicted 10° sectors.

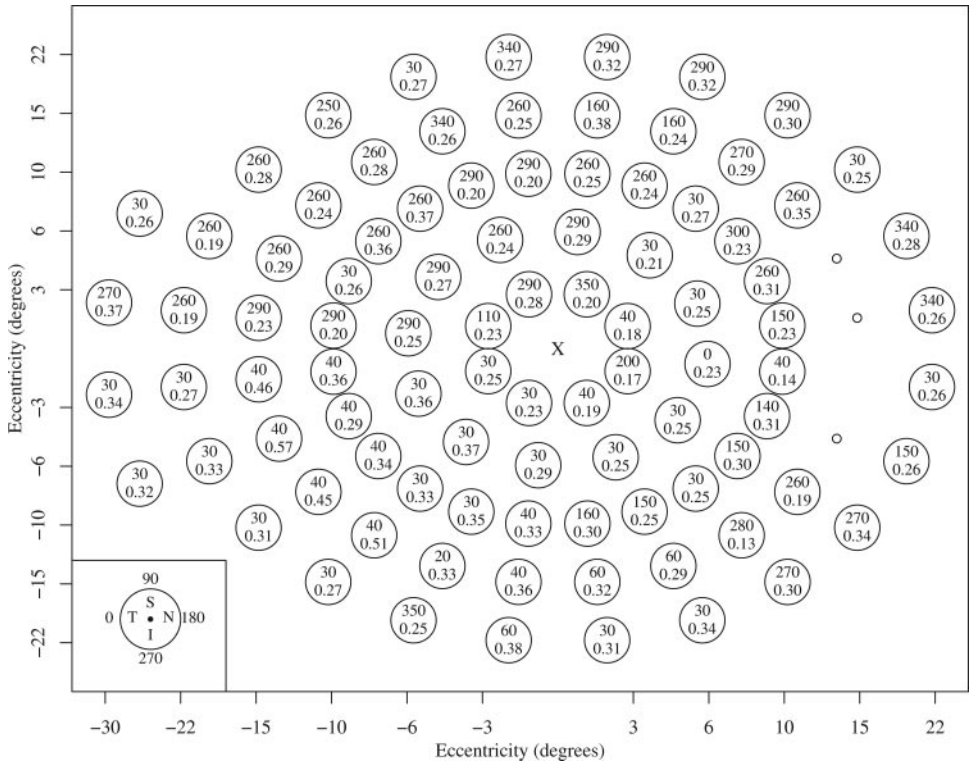

FIGURE 5. The map of visual field location to the ONH computed by using the Basic approach. Each location of the visual field is represented with a circle containing the angle on the ONH for that location (*top of circle*) and the corresponding correlation coefficient. The key in the *bottom left* shows how angles appear on the ONH. Note that axis labels are an indicative, nonlinear scale.

whether the mean correlation coefficients are significantly different, as the data are a mix of paired and nonpaired comparisons, and the data are not statistically independent, hence requiring a complicated analysis that is not readily interpretable.

Adding the constraint that the sector matching to a location must be within 40° of the angle predicted by Algorithm GROW reduces the number of locations covered even further, to only 31% of the field (Table 2, row 3).

Normalizing by the fellow eye increases the number of locations with statistically significant correlations, raising coverage of locations to 67%, with little change in the overall correlation coefficients (Table 2, row 4). And finally, using rim volume, rather than rim area reduces coverage slightly to 59%. The *z*-test on proportions reveals that it is unlikely that the increase in the number of locations covered when normalizing by the fellow eye is due to chance ($z = 4.84$, $P < 0.001$ for Fellow-A, and $z = 3.75$, $P < 0.001$ for Fellow-V). Figure 6 shows the two maps for the Fellow-A and -V methods.

TABLE 2. Number of Statistically Significant Correlations and the Range of Correlation Coefficients for Each Method

	Number of Locations	Percentage of Locations	Correlation Coefficients		
			Min	Max	Mean
Basic	90	96	0.13	0.57	0.29
Basic-p	50	53	0.26	0.57	0.33
Basic-pg	29	31	0.26	0.57	0.34
Fellow-A	63	67	0.27	0.52	0.36
Fellow-V	55	59	0.27	0.54	0.35

The Basic method had less than 100% coverage, because only positive correlations were counted.

DISCUSSION

This article presents a partial structure–function map for data obtained from the Medmont perimeter that is summarized in Figure 7. Perhaps more important, the novel contribution of this work is the methodology by which this map was derived. The methods build on previous work by Anton et al.,[6] and subsequently Gardiner et al.,[2] that correlate visual field sensitivity at individual locations in the visual field to sectorial optic disc features returned from the HRT. The most novel aspect is the development of the optic nerve growth model GROW that provides a framework for the exclusion of nonanatomically plausible correlations.

Consistent with previous reports, the magnitude of the correlations between ONH parameters and visual sensitivity is low. There are numerous reasons why this is likely when pooling data across individuals. First, there is considerable anatomic variation between individuals, for example, in the position of the ONH relative to the horizontal meridian and in axial length. Second, there is noise associated with both the HRT measures and measures of visual sensitivity; hence, the parameter estimates are unlikely to be accurate in some individuals. For visual sensitivity, sources of noise include patient error, inattention, and fatigue. Visual field testing inaccuracy also occurs because of the necessary brevity of test algorithms, with bias being introduced by some procedures being influenced by sensitivity outcomes of neighboring points or from prior knowledge of likely sensitivity outcomes represented in the population.[16,17] It is also imperative to keep in mind that the HRT does not provide a direct measure of retinal ganglion cell loss, which would presumably be more directly related to visual field sensitivity. Finally, the present study compares data collected cross-sectionally and therefore assumes that HRT parameters and visual field sensitivity change concurrently—an assumption that is unlikely to be valid.

In this study we chose to use outcomes from the Medmont perimeter as the functional measure. We chose the Medmont

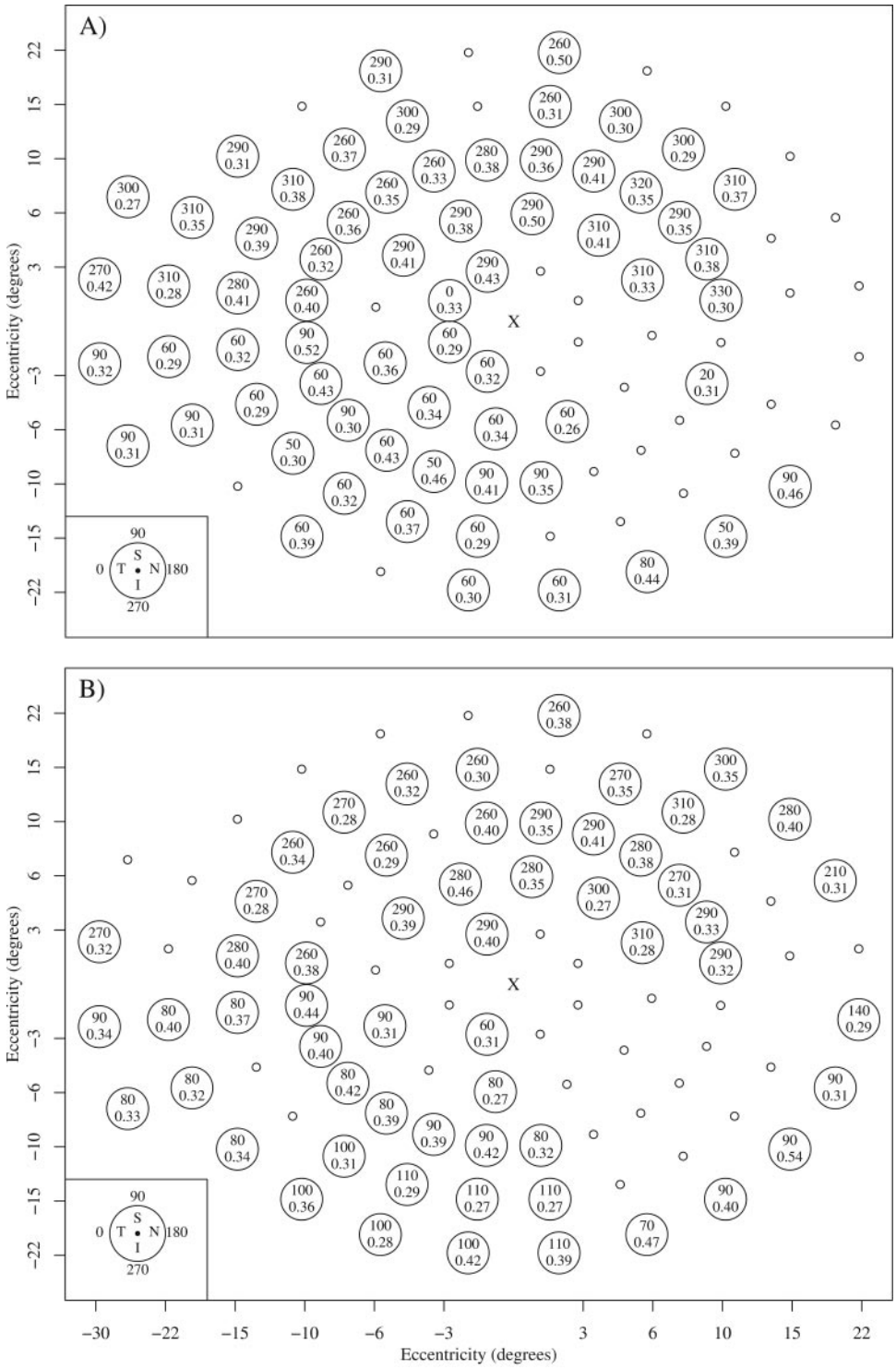

FIGURE 6. The map of visual field location to the ONH computed using (**A**) the Fellow-A and (**B**) Fellow-V approaches. Numbers are as described in Figure 5.

rather than the better-known HFA, as the Medmont samples significantly more locations in the arcuate regions of the visual field than the HFA. Testing more locations has the potential to introduce larger error in sensitivity estimates due to fatigue and inattention; however, it should be noted that the test duration of the Medmont is only marginally (approximately 10%) longer than that of SITA-Standard. The other main difference between the HFA and the Medmont is the background illumination (31.5 apostilbs for the HFA compared to 10 apostilbs for the Medmont), which results in the dB scaling of the stimuli representing different absolute stimulus luminance levels for the two perimeters. These differences may result in some divergence between our results and previously published maps obtained using HFA data; however, the results should be expected to be largely similar.

In reports of previous studies in which the relationship between visual field sensitivity and structural parameters (either in the form of imaging data, or predicted numbers of ganglion cells responding to perimetric stimuli) was explored, there has been debate regarding whether these parameters are related in a linear or nonlinear fashion.[13,18–20] Consequently, it has been suggested that it may be advantageous to convert

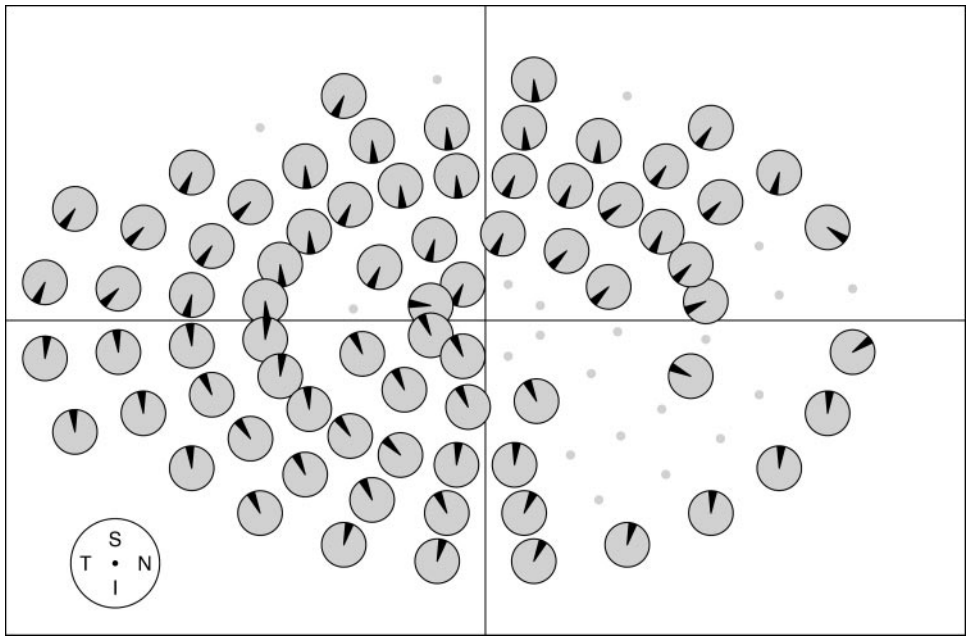

FIGURE 7. A map using both the Fellow-A and -V approaches. Each pie is at a Medmont field location, and the wedge represents the 10° sector with highest correlation coefficient restricted by GROW. When both Fellow-A and -V provided a correlation coefficient for a location–sector pair, the mean was taken before computing the maximum sector. As indicated, temporal (T) ONH is to the *left*.

visual field data to a linear scale when exploring the relationship between visual field sensitivity and structural parameters.[13] This study, however, uses a rank correlation between rim area/volume data and sensitivities measured in dB, and so any order-preserving transform such as linearization of the sensitivity data, would have no effect on our results. We confirmed this by running method Fellow-V after transforming the sensitivity data to a linear scale, and indeed there was no change in the angles produced or in the correlation coefficients from those shown in Figure 6. Hood and Kardon[13] also used a bilinear model that allows for the presence of a non-zero structural measurement in eyes with no function, but none of our participants had advanced loss, and so we did not use this feature when computing correlations.

Our main results relate 10° sectors of the ONH to individual visual field locations. The choice of 10° was quasi-arbitrary—primarily to allow direct comparison with the method used by Gardiner et al.[2] In their structure–function map Garway-Heath et al.[1] used much larger sectors (60–110°). They state that one of the justifications for large sector size is individual anatomic variability in the ONH positions mapped to visual field data. Given anatomic differences, in addition to measurement variability of both visual field and imaging data, there may be some benefit in applying spatial smoothing to the structural or functional data. We explored this issue by testing larger optic nerve sectors (20–30°; Table 3) and found that the number of visual field locations that were significantly related to any of the larger ONH sectors was lower than when 10° sectors were used. A possible explanation for this observation is that taking larger optic nerve sectors resulted in a loss of local defect information. Of course, there are also fewer points; hence, the probability of obtaining statistically significant correlations due to chance is also reduced. We did not explore averaging the visual field data (for example across rings of the Medmont pattern, or more complex spatial filtering[21]); however, smoothing is expected to result in a loss of information arising from localized defects.

Another reason that Garway-Heath et al.[1] chose very large sectors for their final map is that the Humphrey Field Analyzer pattern used to generate the map samples significantly more points that correspond to the superior and inferior poles of the ONH than the nasal and temporal poles. The GROW model shows that this larger sample is also true of the Medmont pattern (as in Figs. 5, 6). As noted by Garway-Heath et al.,[1] this sampling method results in enhanced ease of clinical detection of visual field defects due to superior and inferior optic nerve focal loss relative to nasal and temporal changes. Most criteria for glaucomatous visual field loss require a cluster of points to have abnormal sensitivity. If field loss arises from focal loss not at the inferior and superior poles, it is difficult to get a cluster of points with existent visual field patterns (hence these individuals are likely to remain classified as suspects). In an attempt to capture some of these individuals, we included both those

TABLE 3. Number of Locations with Statistically Significant Correlations ($P < 0.05$) Using Different Sector Sizes, Normalizing with the Fellow Eye

	Degrees in Sector	Deviation from GROW	Number of Locations	Correlation Coefficients		
				Min	Max	Mean
Rim Area	10	±4	63 (67%)	0.27	0.52	0.36
	20	±2	46 (49%)	0.26	0.47	0.35
	30	±1	40 (43%)	0.26	0.49	0.35
Rim Volume	10	±4	55 (59%)	0.27	0.54	0.35
	20	±2	42 (45%)	0.27	0.49	0.34
	30	±1	38 (40%)	0.27	0.47	0.34

The third column shows the deviation allowed from the sector predicted by GROW in sectors.

with suspected glaucoma and those with diagnosed glaucoma in our study.

Approximately 33% of the visual field points were not significantly related to any of the optic nerve sectors in our patient set. Our sample size was relatively small, although of a similar size, or larger than several other works relating structure to function.[1,5–7] As discussed herein, current clinical approaches may make it difficult for patients with nasal/temporal focal loss due to glaucoma to be detected, if they exist. Alternately, perhaps the locations not mapped are not of interest in the majority of patients with glaucoma. To explore these questions, future studies could use information regarding the relationship between structure and function information to more accurately and efficiently direct visual field testing.

Indeed, our model GROW can be used to develop visual field testing maps for individuals that relate to specific optic nerve features. Although the presentation of the GROW model presented herein is fairly simplistic and is based on population average data, a potential powerful benefit is the customization of the growth pattern for individual anatomic variation. For example, the location of the ONH relative to the horizontal meridian, axial length, and even the RNFL profile, if it is measured before the onset of the disease process, can all be incorporated to develop an individual structure–function map. Future research is needed to determine the utility of this potentially powerful tool for guiding customized visual field assessment, particularly for longitudinal follow-up.

Acknowledgments

The authors thank Ted Garway-Heath for informative discussions.

References

1. Garway-Heath DF, Poinoosawmy D, Fitzke FW, Hitchings RA. Mapping the visual field to the optic disc in normal tension glaucoma eyes. *Ophthalmology.* 2000;100(10):1809–1815.
2. Gardiner SK, Johnsonn CA, Cioffi GA. Evaluation of the structure-function relationship in glaucoma. *Invest Ophthalmol Vis Sci.* 2005;46(10):3712–3717.
3. Bowd C, Zangwill LM, Medeiros FA, et al. Structure-function relationships using confocal scanning laser ophthalmoscopy, optical coherence tomography, and scanning laser polarimetry. *Invest Ophthalmol Vis Sci.* 2006;47:2889–2895.
4. Schiefer U, Benda N, Dietrich TJ, Selig B, Hofmann C, Schiller J. Angioscotoma detection with fundus-oriented perimetry. a study with dark and bright stimuli of different sizes. *Vision Res.* 1999; 39(10):1897–1909.
5. Weber J, Ulrich H. A perimetric nerve fiber bundle map. *Int Ophthalmol.* 1991;15(3):193–200.
6. Anton A, Yamagishi N, Zangwill L, Sample PA, Weinreb RN. Mapping structural to functional damage in glaucoma with standard automated perimetry and confocal scanning laser ophthalmoscopy. *Am J Ophthalmol.* 1998;125(4):436–446.
7. Yamagishi N, Anton A, Sample PA, Zangwill L, Lopez A, Weinreb RN. Mapping structural damage of the optic disk to visual field defect in glaucoma. *Am J Ophthalmol.* 1997;123(5):667–676.
8. Hawker MJ, Vernon SA, Ainsworth G, Hillman JG, MacNab HK, Dua HS. Asymmetry in optic disc morphometry as measured by Heidelberg Retina Tomography in a normal elderly population: the Bridlington Eye Assessment Project. *Invest Ophthalmol Vis Sci.* 2005;46(11):4153–4158.
9. Levine RA, Demirel S, Fan J, Keltner JL, Johnson CA, Kass MA, Ocular Hypertension Treatment Study Group. Asymmetries and visual field summaries as predictors of glaucoma in the ocular hypertension treatment study. *Invest Ophthalmol Vis Sci*. 2005; 47(9):3896–3903.
10. Oster SF, Deiner M, Birgbauer E, Sretavan DW. Ganglion cell axon pathfinding in the retina and optic nerve. *Semin Cell Dev Biol.* 2004;15(1):125–136.
11. Bowd C, Weinreb RN, Williams JM, Zangwill LM. The retinal nerve fiber layer thickness in ocular hypertensive, normal, and glaucomatous eyes with optical coherence tomography. *Arch Ophthalmol.* 2000;118(1):22–26.
12. Curcio CA, Allen KA. Topography of ganglion cells in human retina. *J Comp Neurol.* 1990;300:5–25.
13. Hood DC, Kardon RH. A framework for comparing structural and functional measures of glaucomatous damage. *Prog Retin Eye Res.* 2007;26(6):688–710.
14. Vingrys AJ, Helfrich KA. The Opticom M-600: a new LED automated perimeter. *Clin Exp Optom.* 1990;73:3–17.
15. Landers J, Sharma A, Goldberg I, Graham S. A comparison of global indices between the Medmont Automated Perimeter and the Humphrey Field Analyzer. *Br J Ophthalmol.* 2007;91(10):1285–1287.
16. Turpin A, McKendrick AM, Johnson CA, Vingrys AJ. Properties of perimetric threshold estimates from Full Threshold, ZEST and SITA-like strategies as determined by computer simulation. *Invest Ophthalmol Vis Sci.* 2003;44(11):4787–4795.
17. McKendrick AM, Turpin A. Combining perimetric suprathreshold and threshold procedures to reduce measurement variability in areas of visual field loss. *Optom Vis Sci.* 2005;82(1):43–51.
18. Garway-Heath DF, Caprioli J, Fitzke FW, Hitchings RA. Scaling the hill of vision: the physiological relationship between light sensitivity and ganglion cell numbers. *Invest Ophthalmol Vis Sci.* 2000; 41:1774–1782.
19. Swanson WH, Felius J, Pan F. Perimetric defects and ganglion cell damage: interpreting linear relations using a two-stage model. *Invest Ophthalmol Vis Sci.* 2004;45:466–472.
20. Hood DC, Anderson SC, Wall M, Kardon RH. Structure versus function in glaucoma: an application of a linear model. *Invest Ophthalmol Vis Sci.* 2007;48:3662–3668.
21. Gardiner SK, Crabb DP, Fitzke FW, Hitchings RA. Reducing noise in suspected glaucomatous visual fields by using a new spatial filter. *Vision Res.* 2004;44:839–848.